4

Crystal Structure of 3d-4f Oxides

3d-4f has the perovskite -like structure, where a perovskite is any material with the same type of crystal structure as calcium titanium oxide ($CaTiO_3$, known as the *perovskite structure*. Perovskites take their name from this compound, which was first discovered in the Ural mountains of Russia by Gustav Rose in 1839 and is named after Russian mineralogist, L. A. Perovski (1792-1856). The general chemical formula for perovskite compounds is ABX_3, where 'A' and 'B' are two cations of very different sizes, and X is an anion that bonds to both. The 'A' atoms are larger than the 'B' atoms.

The correlation between the electronic and magnetic transport and the crystal structure is very important topics. Study crystal structure will help us to understand very interesting physical phenomena represented by these materials. Crystal structure in the present review has been studied using different technique; X-ray diffraction, neutron diffraction and Raman scattering.

4.1 X-ray Diffraction

Crystal structure of europium manganites was investigated using X-ray diffraction and reported in ref [13]. A distorted orthorhombic crystal structure is noted in europium manganites. It was found that the $Eu_{0.65}$ $Sr_{0.35}$ $Mn_{1-x}Fe_xO_3$ samples with x = 0.1, 0.5 and 0.7 consist of one phase single perovskite of orthorhombic system that matched with the ICDD card No. (82-1474). The X-ray diffraction patterns of all samples were refined using Rietveld method to calculate the accurate unit cell dimensions, using the space group P_{bnm}, Z = 4 with A site cations (Sr/Eu) situated at Wyckoff position 4c (x, y, 1/4), B-site cations (M = transition metal cations Mn and/or Fe) situated at Wyckoff position 4b (0.5, 0, 0) and two oxygen atoms O1 and O2 situated at 4c and 4d Wyckoff positions, respectively. A full profile analysis included a refinement of background, scaling factor, lattice parameters, Brag peak profile, positional and thermal parameters were done. The overall good agreement between the

calculated and observed patterns for $Eu_{0.65}Sr_{0.35}Mn_{1-x}Fe_xO_3$, x = 0.1, 0.5 and 0.7 is illustrated in Fig. 4.1. The agreement factors show that the refinement procedures are acceptable for all samples. All the crystallographic data obtained after the refinement of the structure of the investigated samples are summarized and reported in ref. [13]. It is obviously that the volume of unit cell is increased with increasing the iron contents. This small increase seems to be due to the difference between the ionic radii of iron (Fe^{+3} = 0.55Å) and manganese (Mn^{+4} = 0.53 Å). The mean bond length of M – O increases linearly with increasing the iron content x in the $Eu_{0.65}Sr_{0.35}Fe_x\ Mn_{1-x}O_3$ samples. This increase in bond length may explain the increase in the resistivity of the $Nd_{0.65}Sr_{0.35}Fe_xMn_{1-x}O_3$ with the increase in the iron content as reported by Abdel-Latif *et al.* [3]. The octahedral tilt of the perovskite structure has a significant meaning, which describes the charge and magnetic transfer.

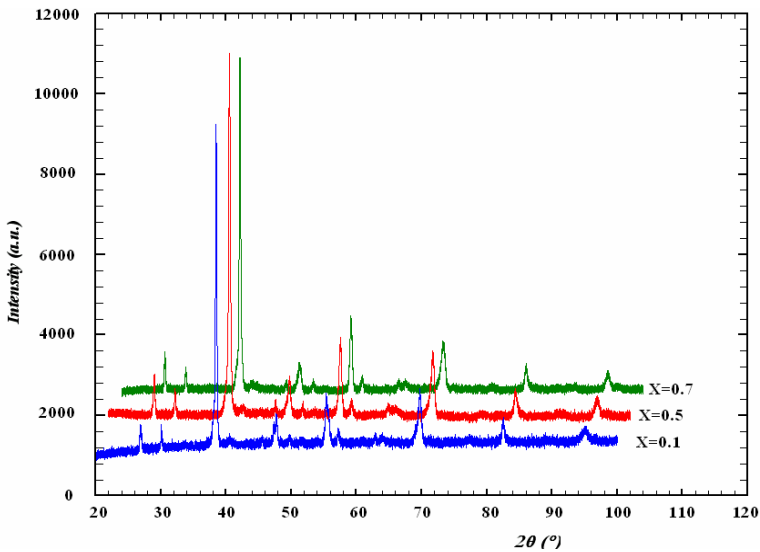

Fig. 4.1 *XRD patterns of the $Eu_{0.65}Sr_{0.35}Fe_x\ Mn_{1-x}O_3$ composite.*

The results of XRD analysis of $Sm_{0.6}Sr_{0.4}MnO_3$ showed that it has an orthorhombic crystal structure of space group *Pnma*. The quality factors of the

acceptable range. The Sm/Sr atoms have (x, 1/4, z) coordinates while the Mn atoms have (0, 0, 1/2) coordinates. Concerning the oxygen atoms; four of them occupy the (x, 1/4, z) coordinates and eight have (x, y, z) coordinates. The x and z of Sm/Sr atoms have the values; 0.0170 and 0.0214 while their values for O (1) atoms are 0.5290 and 0.0310, respectively. The lattice parameters and Mn–O bond lengths of $Sm_{0.6}Sr_{0.4}MnO_3$ in the work presented in ref [20] are compared with those for $Sm_{0.6}Sr_{0.4}MnO_3$ that is prepared in different lab using the same solid state reaction but with different conditions. It is clear that, there is a good agreement between the lattice constants in both samples however, a difference was found only in the bond length of Mn–O. This deviation in the result of the bond length can be attributed to the different values of the octahedral tilting (MnO_6). The tilt of MnO_6 is calculated according to the well-known formula given in Ref. [1]. The tilt angles of the sample under-investigation are [b] tilt ~ 6.8755◦ and [c] tilt ~ 1.05725◦ and they have small values compared with those calculated for $Sm_{0.6}Sr_{0.4}MnO_3$ prepared with different conditions and reported in Ref. [20] namely; [b] tilt ~ 10.65◦ [c] tilt ~ 10◦. This is an indication that in our sample there is less distortion on the MO_6 octahedron than that in the sample. The crystal structure research, here, is one of the most important subjects because of the strong correlation between this crystal structure and electromagnetic transport phenomena as we will see latter.

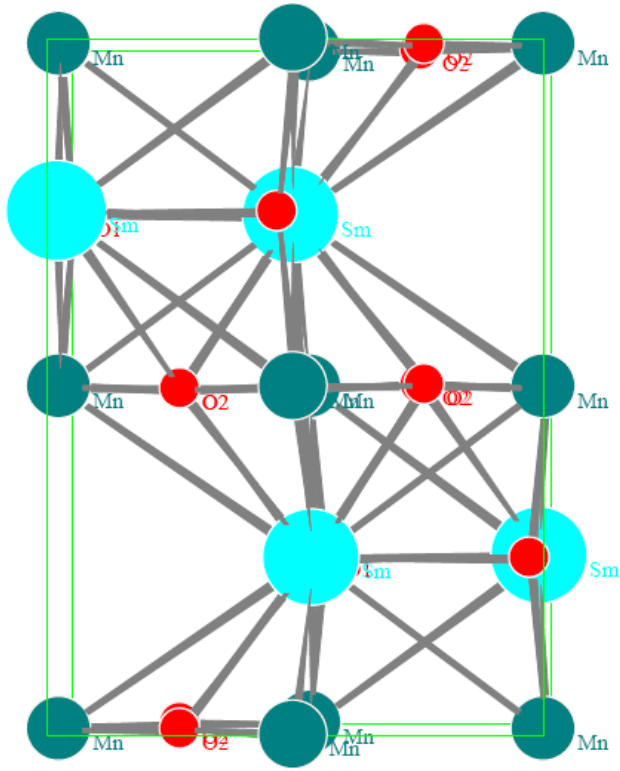

Fig. 4.2 *Crystal structure of $SmSrMnO_3$.*

X-ray diffraction pattern of $Nd_{0.6}Sr_{0.4}Mn_xCo_{1-x}O_3$ composites (x=0 and x=1) which annealed at 850 ℃ for 12h and (x=0.3 and 0.7) annealed at 750 ℃ for, measured at room temperature, is shown in Fig. 4.3. It is quite clear that all reflections are corresponding to the orthorhombic crystal system of space group *Pnma* (No 62). All the reflections which belong to the orthorhombic crystal system of P_{nma} space group for $Nd_{0.6}Sr_{0.4}Mn_xCo_{1-x}O_3$ where x=0.3, and 0.7 are represented in Fig. 4.4. The maximum refection intensity at 121 planes is observed as illustrated in Fig. 4.4. The lattice parameters of this composites resulting from fitting of the experimental XRD pattern using Fullprof program [67] are listed in table 4.1. The crystalline parameters are calculated using the well known Scherrer formula;

$$\text{Crystalline size} = k\lambda/(B \sin\theta)$$

where B is FWHM and equal to $B_{obs.} - B_{std.}$ ($B_{obs.}$ is FWHM of observed sample and B_{std} is FWHM of standard sample).

One can note that the good agreement between the particle sizes deduced from the SEM micrograph and the XRD diffraction.

Table 4.1 *Lattice parameters and volume of unit cell of* $Nd_{0.6}Sr_{0.4}Mn_xCo_{1-x}O_3$.

x	a Å	b Å	c Å	V $Å^3$	Crystalline Size (nm)
0.0	5.227	7.5388	5.4058	213.046	74.8
0.3	5.4479	7.6708	5.4080	225.999	113.5
0.7	5.4417	7.7124	5.4400	228.309	147.4
1.0	5.4285	7.6850	5.4847	228.811	34.2

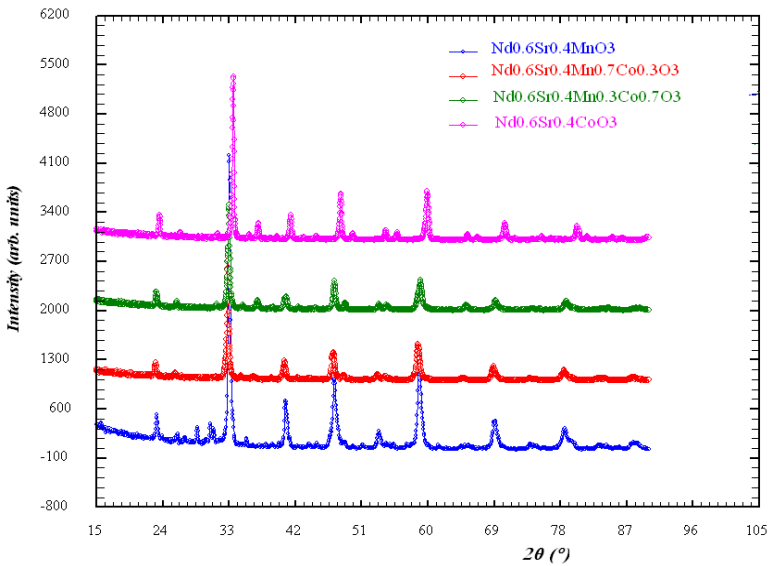

Fig. 4.3 *XRD pattern of* $Nd_{0.6}Sr_{0.4}Mn_xCo_{1-x}O_3$ *(x=0 and x=1) annealed at 850 ℃ for 12h and (x=0.3 and 0.7) annealed at 750 ℃ for 12h.*

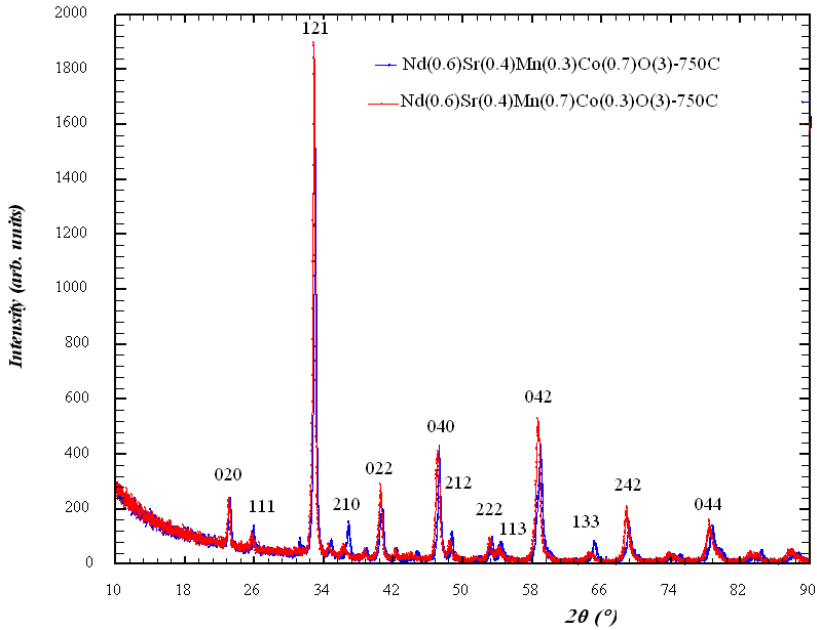

Fig. 4.4 *XRD patterns of $Nd_{0.6}Sr_{0.4}Mn_xCo_{1-x}O_3$ where x=0.3, and 0.7 annealed at 750 ℃ for 12h.*

All XRD patterns of different concentrations of iron in $Nd_{0.65}Sr_{0.35}Fe_xMn_{1-x}O_3$ compounds, measured at room temperature, are displayed in Fig. 4.4. Looking at the observed reflections of the measured XRD it is found that they are corresponding to orthorhombic crystal system.

The refined crystal structure of $Nd_{0.65}Sr_{0.35}Fe_xMn_{1-x}O_3$ phases were deduced by powder X-ray Rietveld analysis. One can say that all compounds crystallize in the orthorhombic structure of space group P*nma* (no. 62). The lattice parameters of $Nd_{0.65}Sr_{0.35}Fe_xMn_{1-x}O_3$ are summarized in Table 4.2. The increase of Iron concentration may lead to decrease in the volume of unit cell. The lattice constants and volume of unit cell for the compounds where x=0.3 and x=0.6 are closed. The lattice parameters of calculated for $Nd_{0.65}Sr_{0.35}Fe_{0.6}Mn_{0.4}O_3$ sample

from XRD are in a good agreement with those calculated by Abdel-Latif et al [24] from neutron diffraction.

Table 4.2 *The lattice parameters of* $Nd_{0.65}Sr_{0.35}Fe_xMn_{1-x}O_3$.

x	*a*, Å	*b*, Å	*c*, Å	V, Å^3
0.1	5.4636	7.7424	5.4662	231.2278
0.3	5.4555	7.7264	5.4595	230.1254
0.6	5.4638	7.7322	5.4595	230.6486

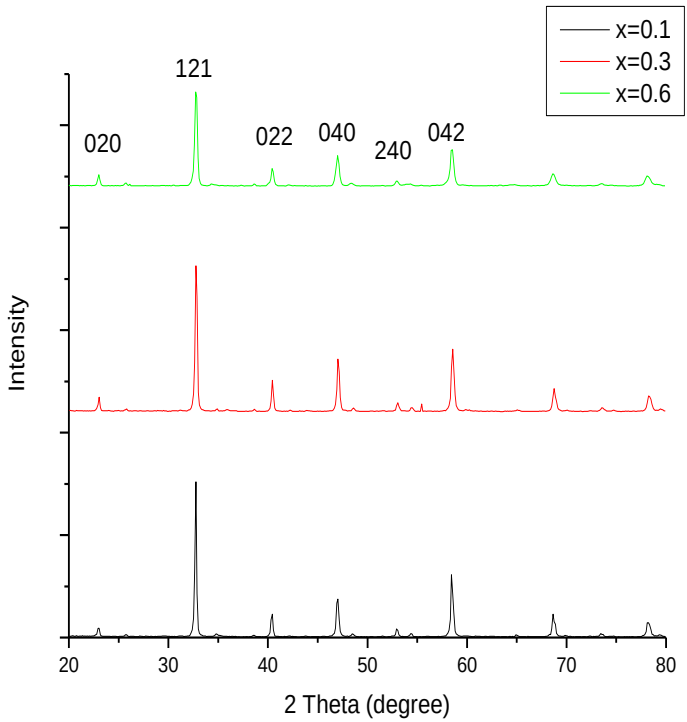

Fig. 4.5 *XRD patterns of different concentrations of iron in* $Nd_{0.65}Sr_{0.35}Fe_xMn_{1-x}O_3$.

Hexagonal crystal structure was observed for ytterbium manganites [17, 21]. X-ray diffraction pattern of the $YbMnO_3$ composite [17] is shown in Fig. 4.6. The XRD of $YbMnO_3$ at different firing temperatures 750 ℃ and 1000 ℃

spectra are refined according to space group $P6_3cm$ where the Yb/Sr atoms occupy two positions *2a* and *4b*. Yb1/Sr1 has (0, 0, 0.2754) and (1/3, 2/3, 0.2274) coordinates while Mn atoms are in 6*c* (0.3518, 0, 0) [22-23]. The fitted lattice parameters of hexagonal crystal system are in a good agreement with those reported by H. A. Salama et al., [24], van Aken et al., [68] Zhoi et al., [69] and Katsufuji et al., [70].

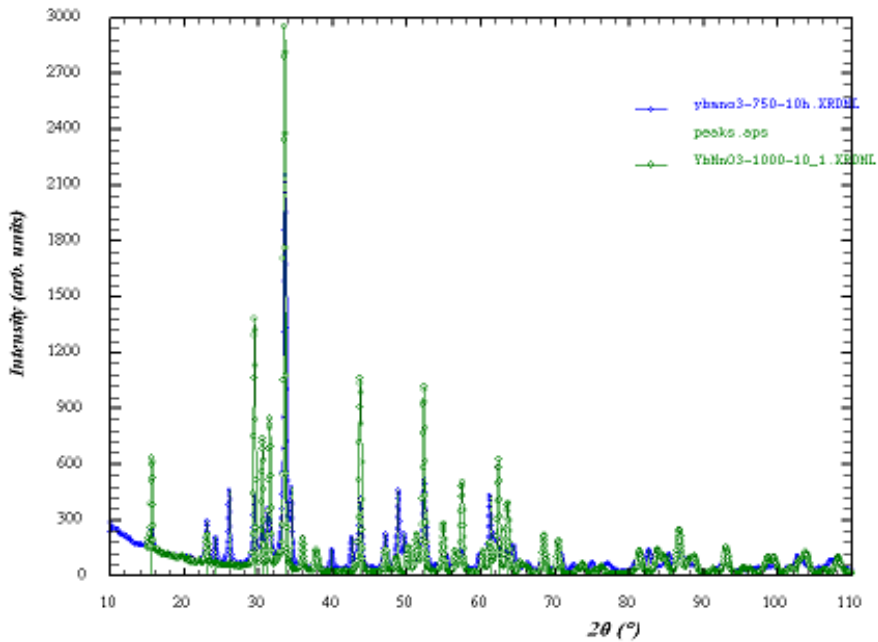

Fig. 4.6 *XRD patterns of the $YbMnO_3$ composite; fired at 1000℃ and at 750℃. The orthorhombic system is refined according to space group Pnma where the Yb/Sr atoms have (x, 1/4, z) coordinates and the Mn atom has (0, 0, ½) coordinates. Concerning the oxygen atoms; four of them occupy the (x, 1/4, z) coordinates and eight have (x, y, z) coordinates. On the other hand the hexagonal system is refined according to space group $P6_3c$. [17].*

The effect of strontium doping on crystal structure is showed in the present review where the diffraction pattern of $Yb_{0.9}Sr_{0.1}MnO_3$ showed that this compound has mixed crystal structure phases (hexagonal and orthorhombic) [17].

4.2 Neutron Diffraction

Neutron diffraction measurements for $Yb_{0.6}Sr_{0.4}MnO_3$ and $Yb_{0.9}Sr_{0.1}MnO_3$ in the temperature range from 2.5K up to room temperature are shown in Fig. 4.7 (a-b). It is noted from the lattice parameters of $Yb_{0.6}Sr_{0.4}MnO_3$ that the volume of unit cell of both hexagonal and orthorhombic depends on the temperature where it increase with decreasing temperature see Fig. 4.7. Neutron diffraction patterns were refined using Fullprof software [76] which based on Rietveld method. According to refinement of neutron diffraction patterns of $Yb_{0.6}Sr_{0.4}MnO_3$ it is found that the crystal structure of $Yb_{0.6}Sr_{0.4}MnO_3$ is possessing mixed orthorhombic/hexagonal phase with space group P*nma* (62) for orthorhombic phase while a space group $P6_3cm$ (185) for hexagonal phase. It is noted from the lattice parameters that the volume of unit cell of both hexagonal and orthorhombic depends on the temperature; increase with decreasing temperature. From the analysis of neutron diffraction patterns of $Yb_{0.9}Sr_{0.1}MnO_3$ it has mixed orthorhombic/hexagonal phase with space group P*nma* (62) for orthorhombic phase while a space group $P6_3cm$ (185) for hexagonal phase as well as in the case of $Yb_{0.6}Sr_{0.4}MnO_3$.

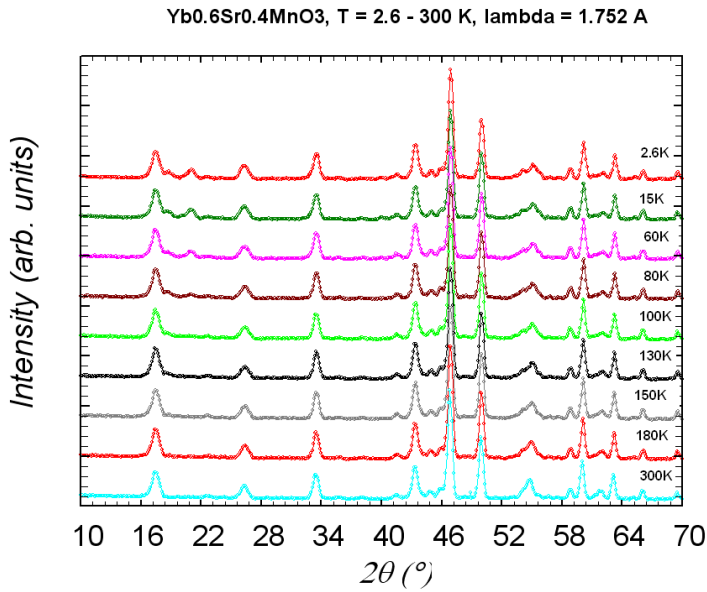

$Yb_{0.9}Sr_{0.1}MnO_3$; T=2.5 – 300K, Lambda =1.752 Å

Fig. 4.7 *The neutron diffraction patterns of $Yb_{0.6}Sr_{0.4}MnO_3$ at different temperatures.*

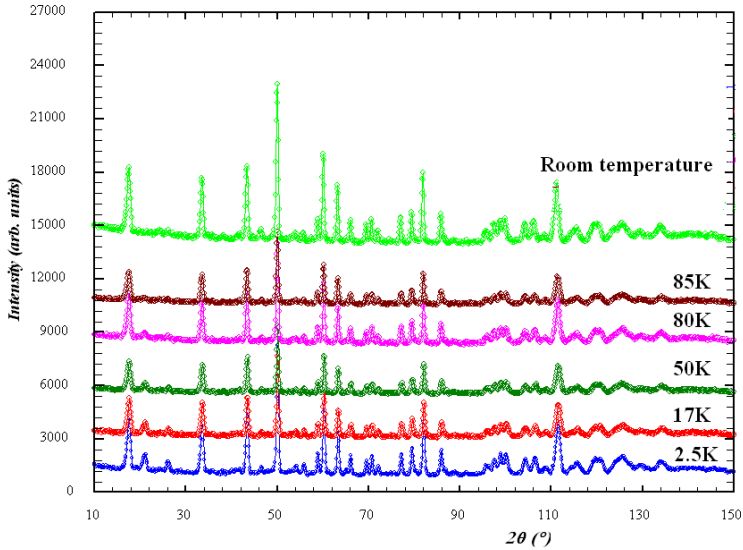

Fig. 4.8 *The neutron diffraction patterns of $Yb_{0.9}Sr_{0.1}MnO_3$ at different temperatures.*

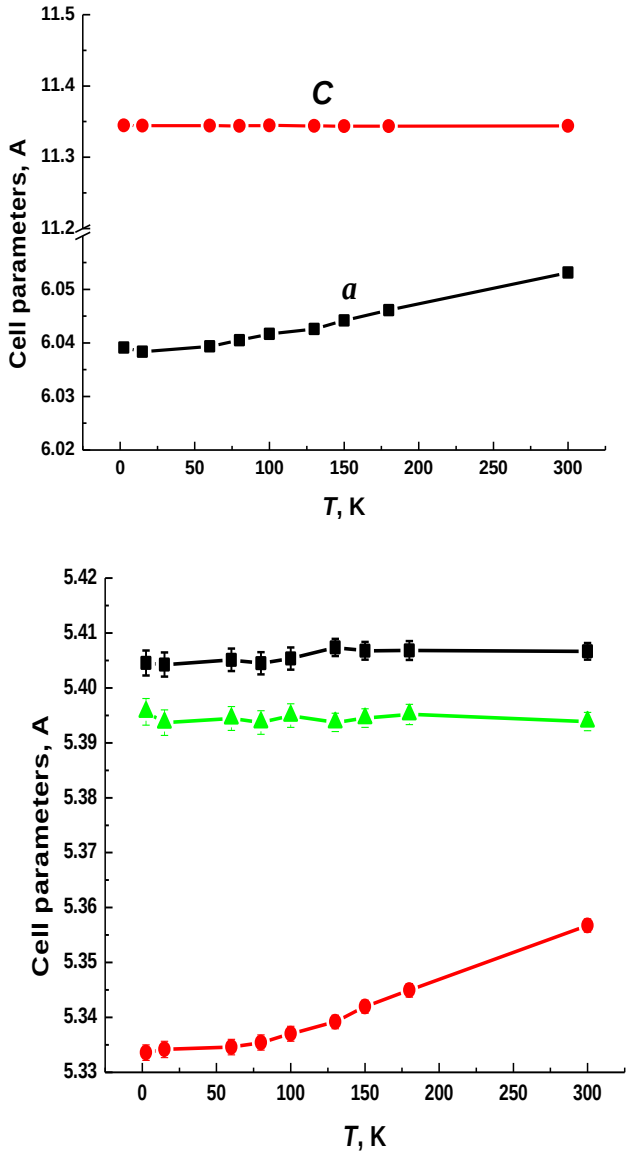

Fig. 4.9 *Lattice parameters of $Yb_{0.6}Sr_{0.4}MnO_3$ of both hexagonal and orthorhombic phases as a function of temperature.*

The neutron diffraction patterns of the $NdFe_{0.6}Mn_{0.4}O_3$ at different temperatures (114 K and 287 K) are showed in Fig. 4.10. The analysis of the magnetic structure, of these diffraction patterns, shows that this compound has non-collinear ordering (weak ferromagnetic ordering) at 114 K. temperature.

The component of magnetic moment at x-, y- and z-axis and the resulting magnetic moment are given in table 4.3. It is clear that the components of magnetic moment in y and z axis are constant with increasing the temperature while the increase only in x-axis. The X-ray diffraction analysis as well as the neutron diffraction and Mössbauer spectroscopy [7] analysis approved the formation of a single phase structure of the samples. The experimentally obtained density of such samples compared with those defined by X-ray is in the range of 88-90%, thus the porosity is of the range 10-12%, (in the acceptable range). The lattice parameters of all samples are given in Table 4.3 and the neutron diffraction pattern of $Nd_{0.65}Sr_{0.35}Mn_{0.4}Fe_{0.6}O_3$ is shown in Fig. 4.7. All spectra are refined according to space group Pnma where the Nd/Sr atoms have (x, 1/4, z) coordinates and the Fe/Mn atoms have (0, 0, ½) coordinates. Concerning the oxygen atoms; four of them occupy the (x, 1/4, z) coordinates and eight have (x, y, z) coordinates. The x and z of Nd/Sr atoms have values from 0.024 and0.002 to 0.071 and 0.033, respectively while their values for O(1) atoms vary from 0.495 and 0.001 to 0.642 and 0.042, respectively. The O(2) atoms coordinates x, y and z are in the range from -0.251, 0.001, 0.221 to -0.345, 0.033, 0.353, respectively. The refined thermal parameters, obtained from the analysis of X-ray diffraction patterns, are anisotropic for all x, see Table 4.3. The quality factors of the refinements are in the range of acceptable values as listed in Table 4.4.

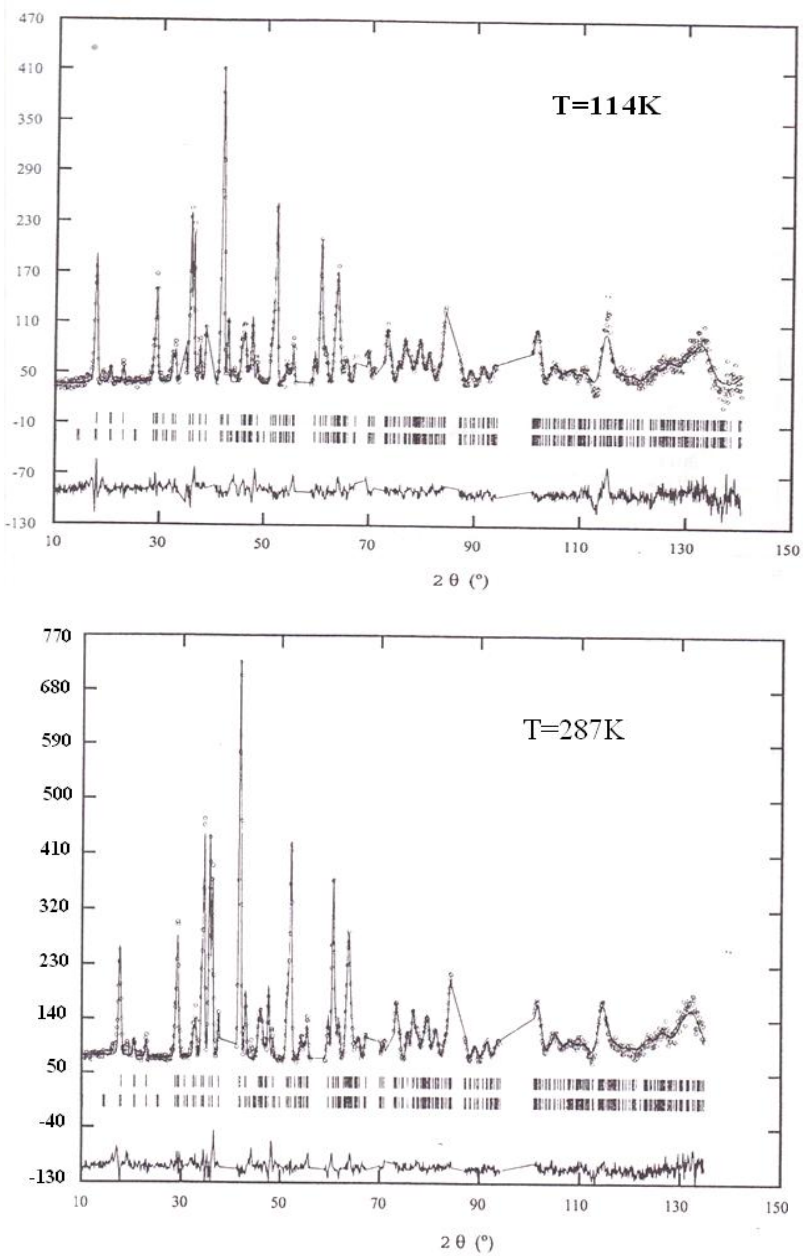

Fig. 4.10 *The neutron diffraction patterns of* $NdFe_{0.6}Mn_{0.4}O_3$ *at different temperatures.*

The obtained lattice parameters, positional and thermal parameters are in a good agreement with those given in the literature for similar compounds [8, 9]. The crystal structure does not change with changing the concentration of iron as all the samples have the same space group.

Table 4.3 *Cell parameters and Volume of* $Nd_{0.65}Sr_{0.35}Mn_{0.4}Fe_{0.6}O_3$.

X	*a*	*b*	*c*	V
0.2	5.4726(9)	7.6776(13)	5.4361(8)	228.406(3)
0.4	5.4527(9)	7.7283(10)	5.4441(8)	229.415(3)
0.6	5.4638(5)	7.7413(6)	5.4560(5)	230.772(2)
0.6*	5.4627(2)	7.7297(2)	5.4573(1)	230.435(1)
0.8	5.4249(14)	7.7210(17)	5.4622(17)	233.406(5)

* neutron diffraction

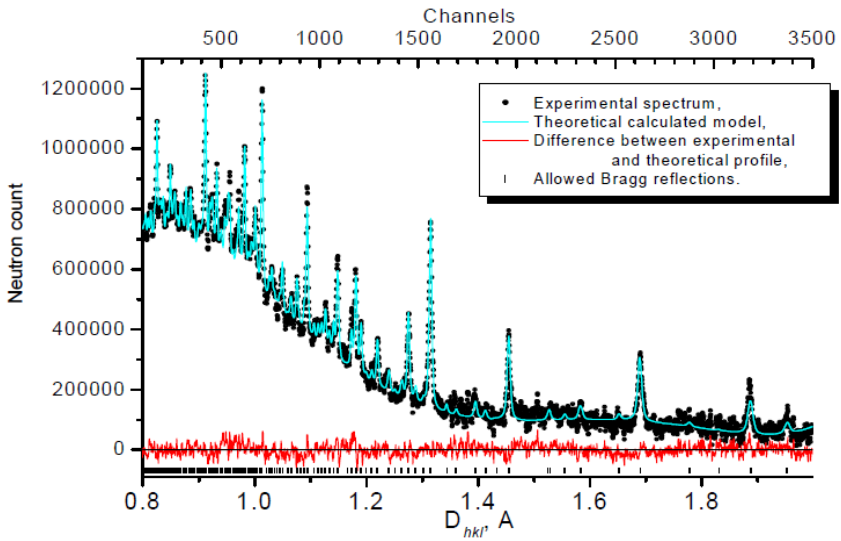

Fig. 4.11 *The neutron diffraction patterns of* $Nd_{0.65}Sr_{0.35}Mn_{0.4}Fe_{0.6}O_3$.

Table 4.4 *Thermal parameters of* $Nd_{0.65}Sr_{0.35}Mn_{0.4}Fe_{0.6}O_3$.

U_{ij}	X	Nd/Sr	Fe/Mn	O1	O2
U_{11}	0.2	0.0305	*0.0121*	*0.0880*	0.0701
	0.4	0.0102	*0.0880*	*0.0354*	0.0657
	0.6	0.0149	*0.0937*	*0.0299*	0.0960
	0.8	0.0106	*0.0601*	*0.0957*	0.0710
U_{22}	0.2	0.0305	*0.0121*	*0.0880*	0.0701
	0.4	0.0102	0.0880	0.1554	0.0657
	0.6	0.0149	0.0937	0.0299	0.0960
	0.8	0.0106	0.0601	0.0957	0.0710
U_{33}	0.2	0.0305	0.0121	0.0880	0.0360
	0.4	0.0102	0.0880	0.1554	0.0327
	0.6	0.0149	0.0937	0.0299	0.0477
	0.8	0.0109	0.0031	0.0470	0.0340
U_{12}	0.2	0	0	0	0
	0.4	0	0	0	0.0058
	0.6	0	0	0	0
	0.8	0	0	0	0
U_{13}	0.2	0.2787	0	0	0
	0.4	-0.0365	0	0	0.0006
	0.6	0	0	0	0
	0.8	0	0	0	-0.0085
U_{23}	0.2	0	0	0	0
	0.4	0	0	0	-0.0038
	0.6	0	0	0	0
	0.8	0	0	0	0

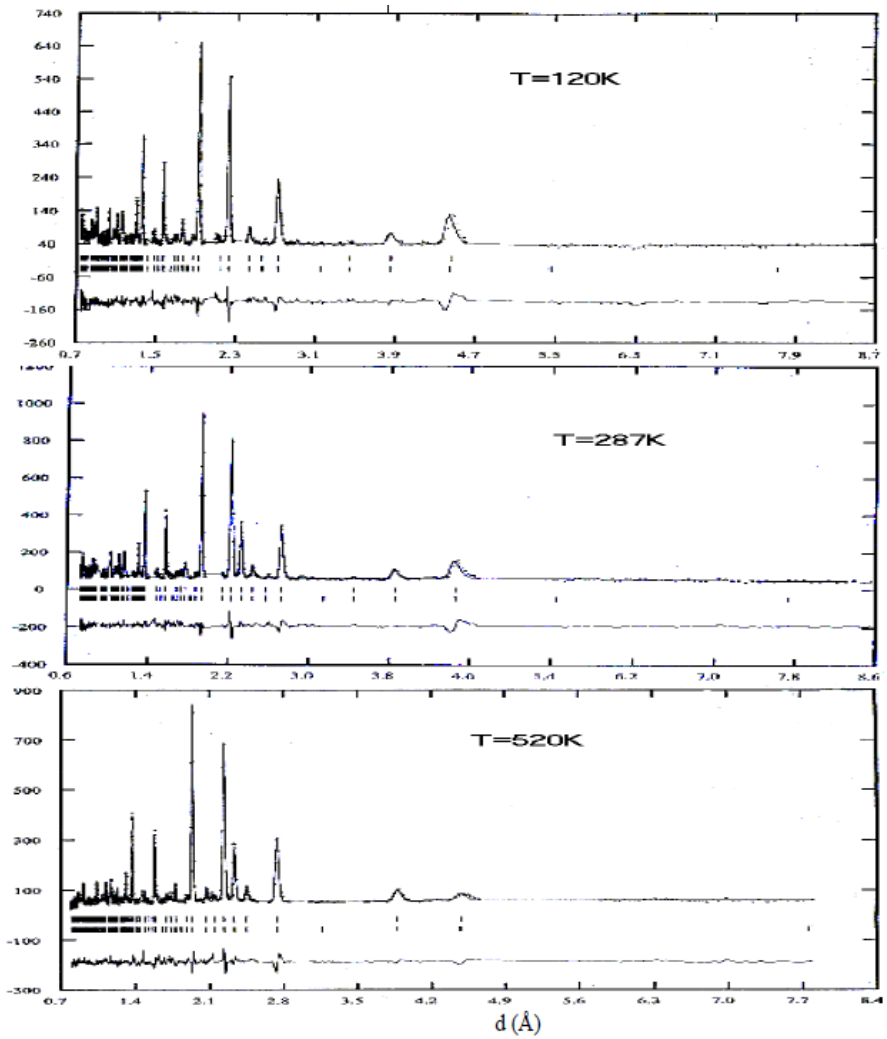

Fig. 4.12 *The neutron diffraction patterns of* $Nd_{0.65}Sr_{0.35}Mn_{0.4}Fe_{0.6}O_3$ *at different temperatures.*

Table 4.5 *The component of magnetic moment for $NdFe_{0.6}Mn_{0.4}O_3$ and $Nd_{0.65}Sr_{0.35}Fe_{0.6}Mn_{0.4}O_3$ at different temperatures.*

T, K	3d-atom	*μ(x)*	*μ(y)*	*μ(z)*	
114	Mn1/Fe1	2.719(40)	0(0)	0.922(127)	$NdFe_{0.6}Mn_{0.4}O_3$
	Mn2/Fe2	-2.719(40)	0(0)	0.922(127)	
	Mn3/Fe3	-2.719(40)	0(0)	0.922(127)	
	Mn4/Fe4	2.719(40)	0(0)	0.922(127)	
287	Mn1/Fe1	2.303(35)	0(0)	0.991(92)	
	Mn2/Fe2	-2.303(35)	0(0)	0.991(92)	
	Mn3/Fe3	-2.303(35)	0(0)	0.991(92)	
	Mn4/Fe4	2.303(35)	0(0)	0.991(92)	
120	Mn1/Fe1	-0.622(0)	0.113(0)	2.541(238)	
	Mn2/Fe2	-0.622(0)	0.113(0)	2.541(238)	
	Mn3/Fe3	-0.622(0)	0.113(0)	2.541(238)	
	Mn4/Fe4	-0.622(0)	0.113(0)	2.541(238)	
287	Mn1/Fe1	-0.622(0)	0.113(0)	2.023(253)	$Nd_{0.65}Sr_{0.35}Fe_{0.6}Mn_{0.4}O_3$
	Mn2/Fe2	-0.622(0)	0.113(0)	2.023(253)	
	Mn3/Fe3	-0.622(0)	0.113(0)	2.023(253)	
	Mn4/Fe4	-0.622(0)	0.113(0)	2.023(253)	
520	Mn1/Fe1	0.740(104)	0(0)	1.0(1)	
	Mn2/Fe2	-0.74 (10)	0(0)	1.0(1)	
	Mn3/Fe3	-0.74 (10)	0(0)	1.0(1)	
	Mn4/Fe4	0.740(104)	0(0)	1.0(1)	

Table 4.6 *The Fe-O bond length for $Nd_{0.65}Sr_{0.35}Fe_xMn_{1-x}O_3$.*

X	0.2	0.4	0.6	0.8
Fe-O_1	1.9954	1.9347	1.9451	1.9413
Fe-O_2	1.7124	1.7704	1.2207	1.4931
Fe-O_2	2.2182	2.1164	3.2971	4.3408
<Fe-O1>	1.9753	1.9754	2.1543	2.5917

The neutron diffraction patterns of the $Nd_{0.65}Sr_{0.35}Fe_{0.6}Mn_{0.4}O_3$ sample, using multi detector diffractometer, at different temperatures (120 K, 287 K and 520 K) are illustrated in Fig. 4.9. The magnetic structure analysis of these diffraction patterns shows that this compound has ferromagnetic character at

120 K and 287 K temperatures. The analysis allows to determine the projections of the magnetic moment at x-, y- and z-axis and the resulting magnetic moment (see Table 4.5). The resulting magnetic moments at 120K and 287 K are 2.6 μB and 2.1 μB, respectively. The projections of the magnetic moment in x and z - directions have the same value and orientation (0.1 μB and –0.6 μB) while there is a difference only in the value of magnetic moment in y-projection where it takes 2.5 μB at 120 K and 1.9 μB at 287 K. In the case of the T =520 K, there is a change in the magnetic ordering where non-collinear magnetic ordering of 1.2 μB resulting magnetic moment is obtained. The projection of magnetic moment in x-axis is equal to zero and in y-axis is equal to 1 μB while in z-axis there are two opposite values ± 0.7 μB between them angle of 73°. From the above, one can say that phase transition, from the pure ferromagnetic ordering into the non-collinear ordering (weak ferromagnetic), occurs near the 520 K temperature.

4.3 Raman Scattering

Raman spectra of $Eu_{0.65}Sr_{0.35}Fe_xMn_{1-x}O_3$ (x=0.1 and 0.5) are shown in Fig. 4.10 and Fig. 4.11, where the frequencies of the experimental peaks of are illustrated. With lower Fe content (x=0.1) in $Eu_{0.65}Sr_{0.35}Fe_xMn_{1-x}O_3$, the spectrum is exhibiting new spectral features. First, the A_{1g} mode is shifted toward lower frequency 210 cm^{-1} compared with A_{1g} in $Eu_{0.6}Sr_{0.4}MnO_3$ which is 238 cm^{-1}, see ref., [29]. With increasing the iron content the A_{1g} mode in x=0.5 is shifted toward higher frequency 216 cm^{-1}. As well as in lower iron concentration the $B_{2g}(1)$ mode is shifted toward lower frequencies, $B_{2g}(1)$ mode shift at frequency equal to 488 cm^{-1}, while it is shifted toward higher frequency 491 cm^{-1} with increasing iron concentration (x=0.5). For $B_{2g}(3)$ mode it is found at frequency equal to 610 cm^{-1} for samples of x=0.1. This $B_{2g}(3)$ mode of Raman spectrum for x=0.5 is shifted to higher frequency than in the case of

x=0.1 to give frequency equivalent to 632 cm^{-1}. The low-frequency mode at 210 cm^{-1} and 216 cm^{-1} have been attributed to the A_{1g} mode, which is the in phase rotation of the oxygen cage about the y-axis to adjacent MnO_6 octahedra. The two high-frequency modes at 488 and 610 cm^{-1} for x=0.1 and at 491 and 632 cm^{-1} for x=0.5) are associated with the out-of-phase bending of the MnO_6 octahedra ($B_{2g}(3)$) and the symmetric stretching of the basal oxygen ions ($B_{2g}(1)$), respectively. According to the Martin–Carron et al. [30], the peak corresponding to $B_{2g}(1)$ mode correlated with the Jahn –Teller distortion for compounds with large ionic radii. The increase in the distortion may lead to the increase of the frequency that is the same in our case the distortion of $Eu_{0.65}Sr_{0.35}Fe_xMn_{1-x}O_3$ increases with increasing the concentration of iron as reported by Farag et al., in ref [13]. The tilt angle increase with increasing the iron concentration. The tolerance factor are the same for both x=0.1 and x=0.5 (t=0.96).

The rare-earth manganites $RMnO_3$ where R with smaller ionic radius like Ho, Er, Tm, Yb, Lu of hexagonal structure and of space group P_{63cm} (C^3_{6v}) with Z=6 can be converted to the orthorohombic phase of space group $Pnma$ (D^{16}_{2h}) with Z=4. The results of group-theoretical analysis for the Γ-point phonons of orthorhombic gives the irreducible representations for the R, Mn and O atoms in the orthorhombic structure that occupy 4(c), 4(b) and 4(c), respectively (they are 12 for each Wyckoff position) [32]. For R atoms $\Gamma = 2A_g + B_{1g} + 2B_{2g} + B_{3g} + A_u + 2B_{1u} + B_{2u} + 2B_{3u}$, for Mn atoms $\Gamma = 3A_u + 3B_{1u} + 3B_{2u} + 3B_{3u}$ and for O atoms in 4(c) position $\Gamma = 2A_g + B_1g + 2B_2g + B_{3g} + A_u + 2B_{1u} + B_{2u} + 2B_{3u}$. For 8(d) oxygen atoms $\Gamma = 3A_g + 3B_{1g} + 3B_{2g} + 3B_{3g} + 3A_u + 3B_{1u} + 3B_{2u} + 3B_{3u}$. From the total 60 Γ-point phonon modes, there are 24 ($7A_g+5B_{1g}+ 7B_{2g} + 5B_{3g}$) are Raman active, 25 ($9B_{1u}+7B_{2u}+9B_{3u}$) are infrared-active, 8($8A_u$) are silent, and 3($B_{1u} + B_{2u}+ B_{3u}$) are acoustic modes [54]. According to Ghosh et al., [55] the

hexagonal rare earth manganites ($RMnO_3$ where R is Y, Yb, Ho or Er of P_{63cm} space group) which contain six formula units per unit cell (Z=6) have 38 Raman active phonon modes ($9A_1$, $14E_1$ and $15E_2$). From Fig. 4.10 one can note that Raman modes of $Yb_{0.6}Sr_{0.4}MnO_3$ and $Yb_{0.9}Sr_{0.1}MnO_3$ may correspond to both hexagonal and orthorhombic symmetries. Raman modes for $Yb_{0.6}Sr_{0.4}MnO_3$ are the observed at frequencies; 156. 178, 471, 526 and 678 cm^{-1} while the observed modes for those of $YMnO_3$ hexagonal structure reported by Yue-Feng [56] we can find the consistency only with the following Raman modes; A_1 (152 cm^{-1}), E_2 (308 cm^{-1}), E_2 (300 cm^{-1}), E_2 (412 cm^{-1}), A_1 (433 cm^{-1}) and A_1 (685 cm^{-1}) see table 4.7. These modes exist in our case but shifted little bit because the difference in the ionic radius of the elements constituent $YMnO_3$ and both $Yb_{0.9}Sr_{0.1}MnO_3$ and $Yb_{0.6}Sr_{0.4}MnO_3$. Comparing the remained modes with those modes belong to the orthorhombic symmetry, like the case given in ref. [34-35] for $NdMnO_3$ of the orthorhombic symmetry, may give interpretation for the coexistence of the hexagonal symmetry with the orthorhombic symmetry in the same time. The hexagonal symmetry are the predominated in both cases but the orthorhombic symmetry in $Yb_{0.9}Sr_{0.1}MnO_3$ is more pronounced than in $Yb_{0.6}Sr_{0.4}MnO_3$.

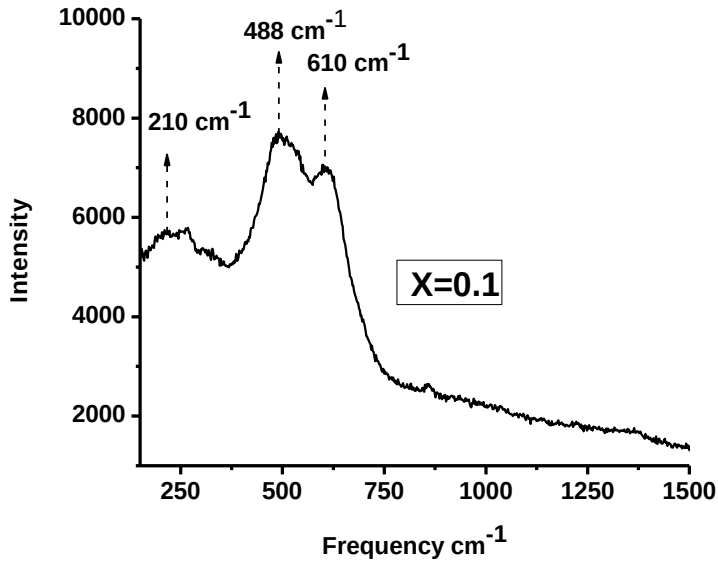

Fig. 4.13 *Raman Spectra of* $Eu_{0.65}Sr_{0.35}Mn_{0.9}Fe_{0.1}O_3$.

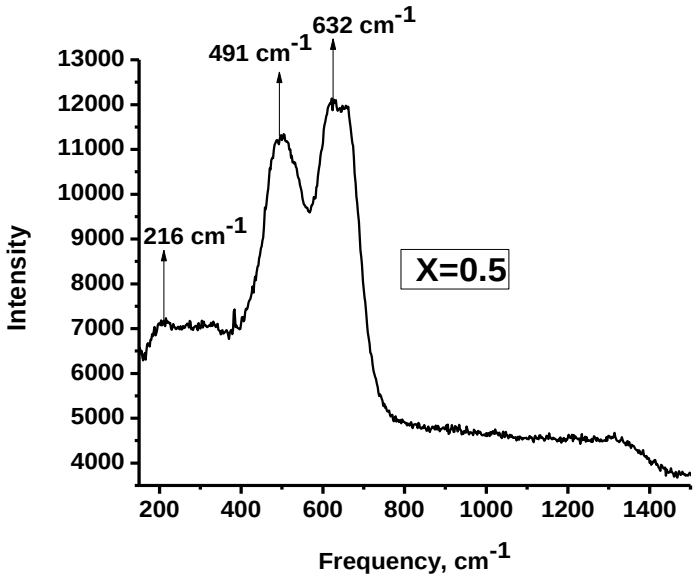

Fig. 4.14 *Raman Spectra of* $Eu_{0.65}Sr_{0.35}\ Fe_{0.5}Mn_{0.5}O_3$.

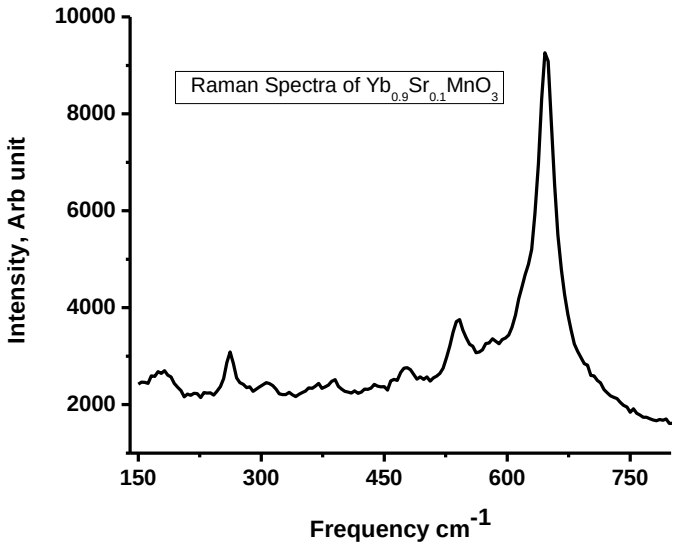

Fig. 4.15 *Raman spectra of both $Yb_{0.6}Sr_{0.4}MnO_3$ and $Yb_{0.9}Sr_{0.1}MnO_3$. $Yb_{0.9}Sr_{0.1}MnO_3$ at the following frequencies; 180, 261, 309, 379, 476, 540, 581 and 645 cm^{-1}. Compared these frequencies with.*

Table 4.7 *Raman modes of $Yb_{0.9}Sr_{0.1}MnO_3$ and $Yb_{0.6}Sr_{0.4}MnO_3$.*

Raman mode	$YMnO_3$	$NdMnO_3$ O	$Yb_{0.9}Sr_{0.1}MnO_3$	$Yb_{0.6}Sr_{0.4}MnO_3$
A1	h 152 [33],		-	156 [21]
Ag	O 151 [31]			
E2	h 300 [34]		309 [21]	-
E2	h 412 [33]		379 [21]	-
A1	h 433 [33]		476 [21]	471 [21]
A1	h 665 [33]		645 [21]	678 [21]
Ag	O 188 [31]	200 [34]	180 [21]	178 [21]
B1g		522 [35]	540 [21]	526 [21]
B3g		282 [35]	261 [21]	-
B2g		601 (23)	581 [21]	-

h = hexagonal and O = orthorhombic